NUMERICAL INVESTIGATION ON BOTTOM GAP OF MICRO FLOW SENSOR

Mohd Zulkiefly Abdullah[1], T. Kouta, Takuma Kamijo[2], Makoto Yamamoto[2*], Shinji Honami[2] and Shoji Kamiunten[3]

Micro sensor is very useful for flow measurements in a number of engineering applications. Especially, it is necessary for the development of MEMS. This paper presents the 3D numerical simulation of flows around a micro flow sensor, which is mounted on a flat plate. The effects of the sensor configuration (i.e. bottom gap) and the Reynolds number on the flow field are numerically investigated. The numerical results indicate that the bottom gap clearly affects the flow fields over the top surface of the sensor. The Reynolds numbers also show a significant influence on the flow nature, especially on the recirculation zone at downstream of the sensor. The present results illustrate a certain improvement on the flow field for the sensor installed at 0.5mm above the wall with four pillars, comparing with that directly mounted on the wall.

Keywords: MEMS, Micro Flow Sensor, Incompressible Flow, Three-Dimensional Computation

1. INTRODUCTION

The measurement of fluid flow is one of essential fields in a sensor technology of process control. Important applications of a flow sensor can be found in mechanical engineering, medical equipment, semiconductor fabrication, automobile industry and so on[1]. Especially, with the recent development of micro-machines, the flow measurement in micro-machines has been a critical issue. In many cases of micro-machines, however, the measurement must take place inside the channel or pipeline having a small cross-sectional area that usually inaccessible with the conventional sensors. Thus, the micro sensor is needed for such purposes, and it must have excellent reliability under severe conditions and have to be realized at low cost.

In recent years, using the MEMS technology, a great number of thermal flow sensors have been fabricated and employed in different applications [2-5]. They have been classified into two types. One is the hot wire anemometer type, where the cooling caused by forced convection is detected. The other is the temperature difference type, where the difference of the temperature between upstream and downstream the micro heaters is detected. In a micro-liquid handling system, one of the basic components is the micro liquid flow sensor, which is made by using the 'time-of-flight' flow sensing technique[7,10]. Other micro-machined flow sensor is also realized in or close to the flow channel for sensing gas flows[4,6,8,9]. They make use of a heater whose temperature is a function of the heat carried away by the medium in the channel.

For the optimal design of a micro sensor, to investigate the flow field around it is important and necessary. However, since a micro flow sensor is so small in scale, it is too difficult to experimentally measure the flow field. Therefore, the use of a computational fluid dynamics (CFD) is needed to understand the flow behaviour around a sensor, particularly near the sensor surface, before the improvement can be made.

In the present study, the three-dimensional simulations using a computational fluid dynamics (CFD) code has been used to investigate the flow field around the sensor at two different

Received: July 15, 2004, Accepted: February 16, 2005.

1 School of Mechanical Engineering, Engineering Campus, Science University of Malaysia 14300 Nibong Tebal, Penang, Malaysia

2 Department of Mechanical Engineering, Tokyo University of Science 1-3 Kagurazaka, Shinjuku-ku, Tokyo 162-8601, Japan

3 Yamatake Corporation 1-12-2, Kawana, Fujisawa, Kanagawa, 251-8522, Japan

* Corresponding author. Email: yamamoto@rs.kagu.tus.ac.jp

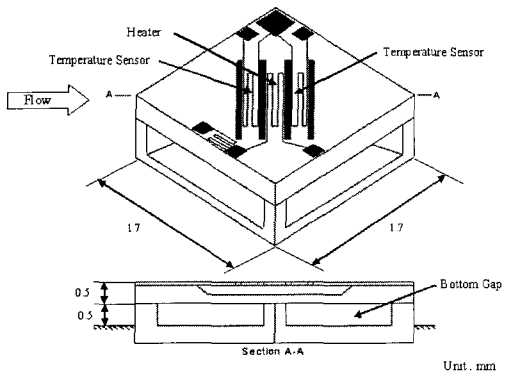

Fig. 1 Micro flow sensor supported with four pillars

installations; (Case A) the sensor is directly mounted on the wall surface and, (Case B) the sensor is installed at 0.5mm above the wall and supported by four square-sectioned pillars. We refer the flow passage below the sensor to "bottom gap". The effects of Reynolds numbers on the flow fields are also studied. The Reynolds numbers are varied from 700 to 7100, considering the practical applications. The numerical results indicate that the flow field over the top surface of the sensor can be significantly improved for the sensor sensitivity, by installing the micro sensor at 0.5mm above the wall.

2. STRUCTURE AND MEASURING PRINCIPLE OF MICRO FLOW SENSOR

The micro flow sensor studied in this study is the temperature difference type. It consists of one heater and two temperature sensors that are thermal sensitive thin films and are fabricated on a silicon chip. Fig. 1 shows the schematic of the micro flow sensor we investigated (Case B). The dimensions of the sensor are 1.7mm, 1.7mm and 0.5mm in width, depth and height, and the bottom gap is 0.5mm. In the operation, electric power is supplied to the heater, to maintain it at a specified temperature higher than that of the surroundings.

The measuring principle of the present micro flow sensor is based on the convective heat transfer from the heated resistance or the upstream sensor to the surrounding fluid. As the fluid flow passes over the micro flow sensor, the asymmetric temperature distribution with respect to the center of the micro flow sensor occurs because of the convective heat transfer. The output signal of the micro flow

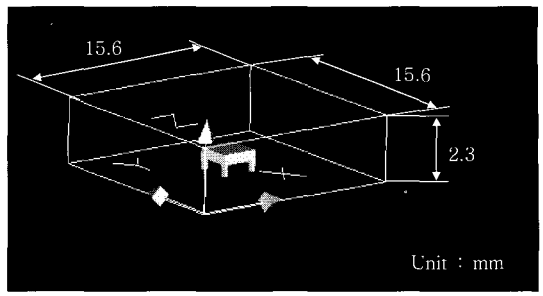

Fig. 2 Model of micro flow sensor with four pillars in a passage

sensor is proportional to the temperature difference between the upstream and downstream temperature sensor. And the flow rate, friction stress and so on can be estimated from this temperature difference. Therefore, larger convective heat transfer (in other words, thinner boundary layer on the top surface, or larger velocity near the sensor) is desirable in the sensor sensitivity and performance. In addition, the flow separation on the sensor top surface should be suppressed to keep stable and accurate measurements.

3. COMPUTATIONAL PROCEDURES

A unit cell containing a micro flow sensor in a rectangular passage is chosen to perform the computational analysis as shown in Fig. 2. Cartesian coordinate is aligned with the edge of the micro sensor, as shown in Fig. 2. In the calculations, the flow is assumed to be incompressible and isothermal. It should be noted that the effect of convective heat transfer from the heater is neglected in the present study.

The governing differential equations used to describe the fluid flow are the Navier-Stokes equations and the equation of continuity as ;

$$\nabla \bullet V = 0 \tag{1}$$

$$\frac{\partial V}{\partial t} + (V \bullet \nabla)V = -\frac{1}{\rho}\mathrm{grad}(P) + \frac{1}{Re}(\Delta V) \tag{2}$$

where Re is Reynolds number. Using the MAC method, the Poisson equation (3) for the static pressure P is derived, by taking divergence of equation (2):

$$\Delta P = -\mathrm{div}(V \bullet \nabla)V + R \tag{3}$$

where

$$R = -\frac{\partial D}{\partial t} + \frac{1}{Re}(\Delta D), \qquad D = \nabla \bullet V \tag{4}$$

and D is a corrective term used to prevent the accumulation of numerical errors. All spatial derivatives except for those of non-linear terms are approximated by 2nd-order central difference. The non-linear terms are discretized by 3rd-order upwind scheme proposed by Kawamura and Kuwahara[11,12];

$$\left(u\frac{\partial u}{\partial x}\right)_i = u_i\left(u_{i+2} - 2u_{i+1} + 9u_i - 10u_{i-1} + 2u_{i-2}\right)/6\Delta x \quad \text{for } u_i > 0 \tag{5}$$

$$\left(u\frac{\partial u}{\partial x}\right)_i = u_i\left(-2u_{i+2} + 10u_{i+1} - 9u_i + 2u_{i-1} - u_{i-2}\right)/6\Delta x \quad \text{for } u_i < 0 \tag{6}$$

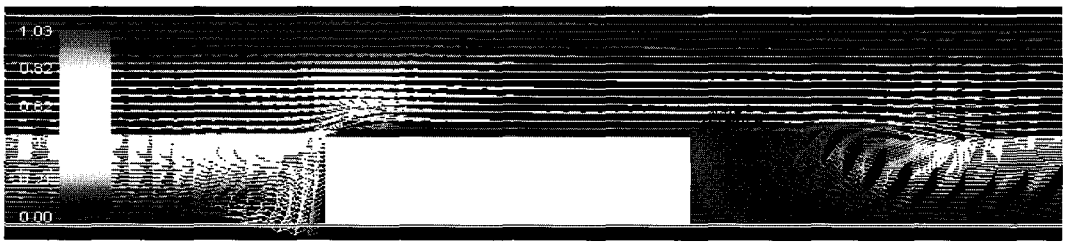

(a) Reynolds No.= 700

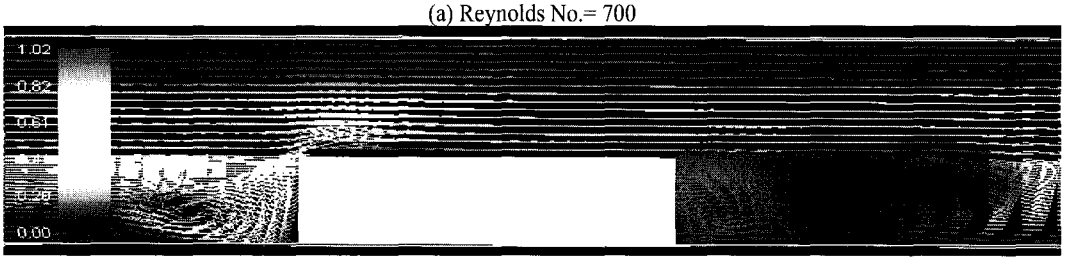

(b) Reynolds No. = 2100

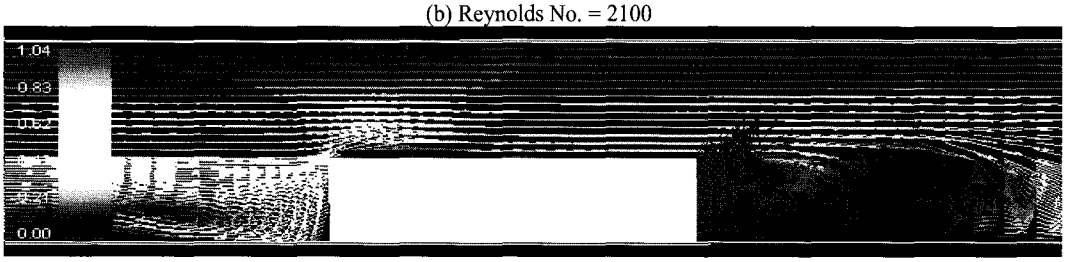

(c) Reynolds No. = 7100

Fig. 3 Velocity vector for the micro flow sensor installed at the wall surface

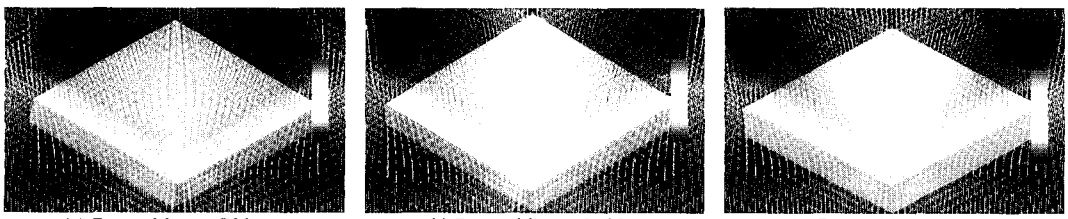

(a) Reynolds no. 700 b) Reynolds no. 2100 (c) Reynolds no. 7100

Fig. 4 Velocity vector on the micro flow sensor top surface

At the inlet boundary, the velocity components of u (x-direction) and v (y-direction) are set to be at the angle of 45° for each coordinate in order to represent the actual measuring position of the micro sensor. The studies are made at Reynolds number of 700 to 7100. These Reynolds numbers are based on the sensor height and the maximum inflow velocity. On the solid surface, all the velocity components and normal pressure gradient are set to be zero. At the outflow boundary, the streamwise gradient of each variable is imposed to be zero. On the top boundary, the normal gradient of each variable is set to be zero.

The computational domain is 15.6mm, 15.6mm and 2.3mm in width, depth and height. This domain size is not large, but sufficient for the present computation, because the flow is completely laminar. The grid system employed in the present numerical analysis has 92, 92 and 81 nodes in the x, y and z-directions respectively (see Fig. 2). A non-uniform grid arrangement in x, y and z directions, with clustering a large number of grid points around the sensor, is used to compute the recirculation zones sufficiently. The code is run on a DELL

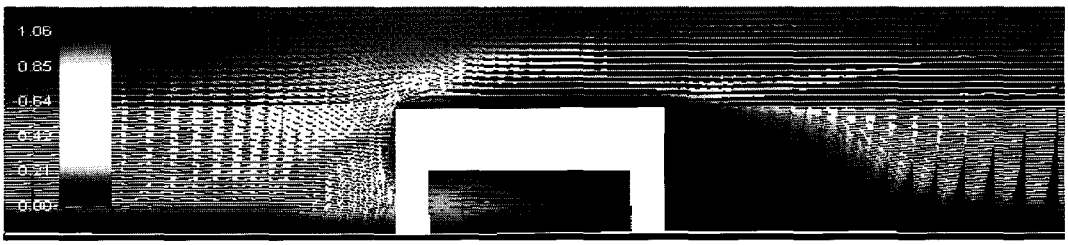

(a) Reynolds No. = 700

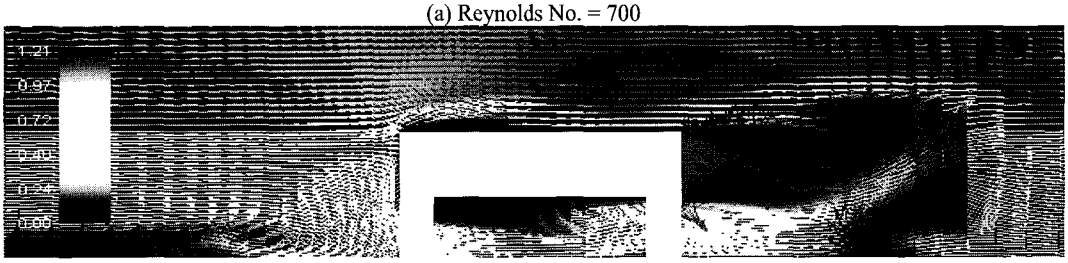

(b) Reynolds No. = 2100

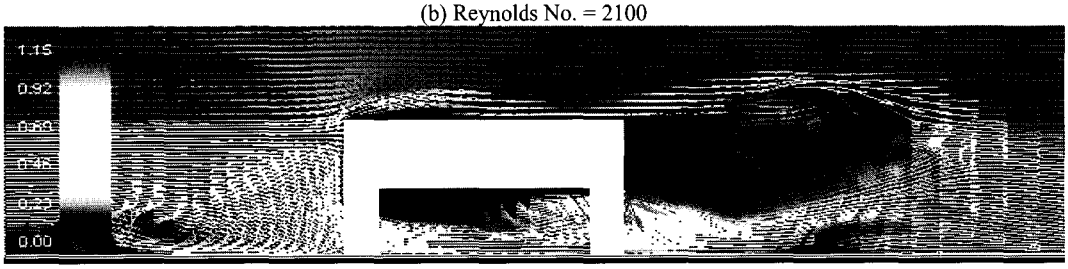

(c) Reynolds No. = 7100

Fig. 5 Velocity vector for the micro flow sensor installed with four pillars

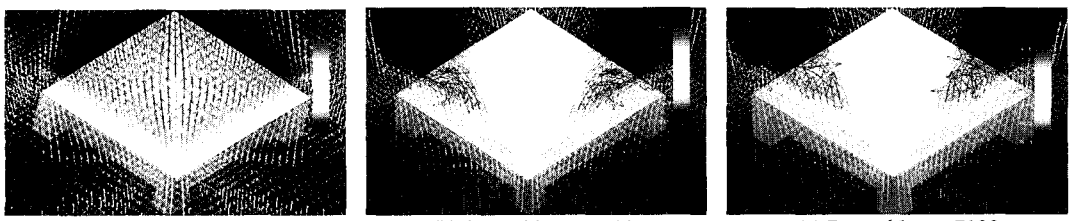

(a) Reynolds no. 700 (b) Reynolds no. 2100 (c) Reynolds no. 7100

Fig. 6 Velocity vector on the micro flow sensor top surface

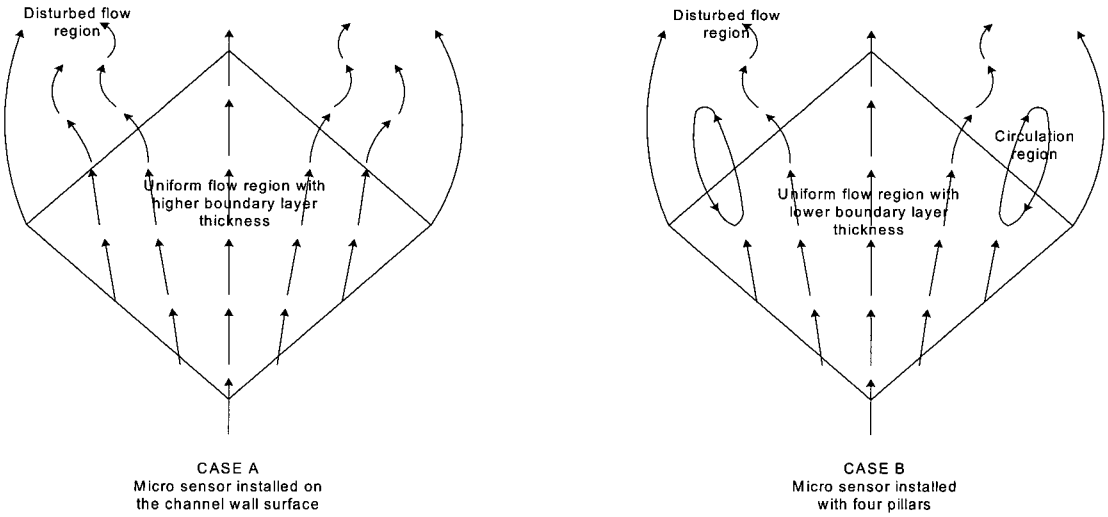

Fig. 7 Schematic diagram of flow pattern on the micro sensor top surface for Case A and B

server with dual Xeon processors 2.8GB speed and with the memory of 2GB. The computation time needed to compute 10000 time steps in this simulation is about 8hours. Time increment Δt was chosen to be 0.001 in all computations.

4. NUMERICAL RESULTS AND DISCUSSION

First, the overall flow nature is investigated for the micro flow sensor directly mounted on the wall (i.e. Case A). We found that the boundary layer flow on the sensor is steady, but the sensor wake is slightly unsteady, that is, it oscillates with very low frequency. The selective results of non-dimensional velocity (i.e. local velocity/freestream velocity) in the diagonal plane are shown in Figs. 3(a) through 3(c) for the Reynolds number of 700, 2100 and 7100. At the Reynolds number of 700 (Fig. 3(a)), the velocity vectors indicate that the flow is relatively smooth. However, a small recirculation is observed at the upstream of micro sensor, whereas at the downstream of sensor a recirculation observed is large just downstream of the micro sensor. It should be noted that the upstream recirculation corresponds to a horseshoe vortex. In Figs. 3(b) and 3(c) for the Reynolds number of 2100 and 7100, the recirculation zones are growing and become more remarkable at the upstream and downstream of the micro flow sensor. The results also indicate that the size of recirculation zone increases with the Reynolds number. Fig. 4(a) shows the bird-eye's view of non-dimensional velocity vectors over the sensor top surface at the Reynolds number of 700. The result demonstrates that the flow velocity over the sensor top surface is drastically reduced into small magnitudes of 0.2 to 0.4 due to the boundary layer effects. It can be seen that the flow is nearly uniform and no vortices are visible. At the higher Reynolds numbers (see Figs. 4(b) and 4(c)), the velocity slightly increases (about 0.21 to 0.41) with the Reynolds number. Moreover, the results illustrate that the flow velocity over the sensor top surface is larger along the diagonal, and smaller towards the left and right corners.

Second, the results for the micro flow sensor with four pillars (Case B) are exhibited. Again, the boundary layer flow on the sensor is steady, but the sensor wake is slightly unsteady. The selective results of non-dimensional velocity vectors are shown in Figs. 5(a) through 5(c) for the Reynolds number of 700, 2100 and 7100. At the smallest Reynolds number (Fig. 5(a)), the velocity vectors show the flow is relatively smooth as similar to Fig. 3(a). However, the recirculation observed just downstream of the micro sensor is much smaller than that of Case A (see Fig. 3(a)). This is caused from the flow passing through the bottom gap of the micro flow sensor. Moreover, we can hardly observe a horseshoe vortex at the upstream of micro flow sensor. In Figs. 5(b) and 5(c) for the Reynolds number of 2100 and 7100, again the recirculation

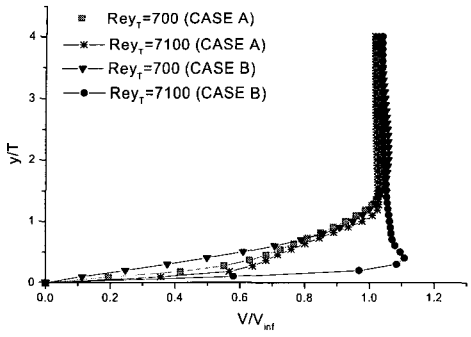

Fig. 8 Velocity profile at the center of micro sensor top Surface

zones are growing and become more visible both upstream and downstream of the micro flow sensor. We can observe that the core of the horseshoe vortex goes away from the micro flow sensor, with increasing the Reynolds number. The result also shows that the flow underneath the micro sensor is increased drastically with the Reynolds number, and this flow with larger velocity has swept the recirculation region downstream of the micro sensor. Thus, the recirculation region has shrunk significantly. Fig. 6(a) plots the bird-eye's view of the non-dimensional velocity vector over the sensor top surface at Reynolds number of 700. The result indicates that the non-dimensional velocity magnitudes are in the range of 0.21 to 0.42, as in Fig. 4(a). Again, the flow is uniform and no vortices are visible. At the higher Reynolds numbers (Figs. 5(b) and 5(c)), the results show that the flow velocities over the sensor top surface are larger at the diagonal, and smaller towards the left and right hand corners. This trend is same as that in Case A. However, the results also indicate that the flows are separated and produced vortices at the left and right hand corners of the micro flow sensor. These flow patterns have drawn in Fig. 7 for clear representation. Taking into account the fact that the velocity at the center region of the top surface are respectively larger than that of Case A (Figs. 4(b) and 4(c)), where the velocities are about 60% higher, these are probably caused by the reduction of the recirculation regions upstream and downstream of the micro sensor. That is, the blockage effect is less effective in the micro sensor with four pillars. From these results and the measuring principle of the micro flow sensor (see Section 2), we can confirm that the larger flow velocity on the sensor top surface in Case B will improve the sensor performance.

Finally, we investigate the characteristic of boundary layer at the center of the sensor top surface. Fig. 8 shows that the boundary layer profiles for both cases and at the three Reynolds numbers. Table 1 lists the effective flow area ratio and the boundary layer thickness. The effective flow area ratio means the ratio of the area where the flow is nearly parallel to the freestream to the total area of the sensor top surface. It is an important parameter for the sensor to measure the flow stably and accurately, and the effective flow area ratio of 100% is the best for the sensor performance. From Fig. 8, it is obvious that the boundary layer thickness is drastically decreased for the micro sensor installed with four pillars (i.e. Case B), especially at the higher Reynolds numbers. As in Table 1, the boundary layer thickness for Case B at the Reynolds number of 700 is about 1.25mm, and is reduced drastically to about 0.2mm at the highest Reynolds numbers. Apparently, the boundary layer thickness in Case B is much smaller than that in Case A. This is because of the less blockage effect of the sensor in Case B. On the other hand, the effective flow area is smaller by about 10% for Case B, compared with those in Case A, for all

Table. 1 Effective area ratio, velocity range and boundary layer thickness on micro sensor top surface at various Reynolds numbers

Reynolds Number	700	2100	7100
CASE A			
1. Effective flow area ratio (%)	100	81	87
2. Boundary layer thickness (mm)	1.18	1.12	1.04
CASE B			
1. Effective flow area ratio (%)	100	73	84
2. Boundary layer thickness (mm)	1.25	0.22	0.22

Reynolds numbers. This is undesirable for the sensor performance. However, since this reduction of effective flow area is caused from the flow separation around the left and right corners, the influence on the sensor sensitivity would be limited.

The overall results obtained here illustrate that the characteristic of the flow over the sensor top surface has improved, by installing the micro sensor with the four pillars.

5. CONCLUSIONS

The effects of the sensor configuration (i.e. bottom gap) and the Reynolds number on the flow field have been predicted by the finite difference method. Three-dimensional computations were performed for two-types of micro flow sensors and at different Reynolds numbers. For the micro flow sensor directly mounted on the wall surface, the boundary layer thickness is larger over the micro sensor top surface. At the higher Reynolds numbers, the recirculation region behind the micro sensor grows with increasing Reynolds number. Therefore, these might deteriorate the sensitivity and performance of the sensor. Meanwhile, for the micro flow sensor installed with four pillars has significantly improved the flow nature around the micro flow sensor, especially the flow over the sensor top surface. This is caused from the flow passing through the bottom gap of the sensor. The boundary layer thickness on the top surface is drastically reduced due to the less blockage effect. Furthermore, the numerical results have shown that the recirculation region behind the micro sensor shrinks, with increasing the Reynolds number. Thorough this study, it was confirmed that the micro flow sensor with four pillars can improve the sensor sensitivity and the performance.

REFERENCES

[1] Berberig, O., Nottmeyer, K., Mizuno, J., Kanai, Y. and Kobayashi, T., 1998, *Sensors and Actuators*, A66, pp.93-98.

[2] Nguyen, N.T. and Kiehnscherf, R., 1995, *Sensors and Actuators*, A 49, pp.17-20.

[3] Pan, T., Hyman, D., Mehregany, M., Reshotko, E. and Garverick, S., 1999, *AIAA Journal*, Vol. 37, No. 1, pp.66-71.

[4] Fang, Q., Chetwynd, D.G., Cavington, J.A., Toh, C.S. and Gardner, J.W., 2002, *Sensors and Actuators*, B 84, pp.66-71.

[5] Ashauer, M., Glosch, H., Hedrich, F., Hey, N., Sandmaier, H. and Lang, W., 1999, *Sensors and Actuators*, 73, pp.7-13.

[6] Neda, T., Nakamura, K. and Takumi, T., 1996, "A poly-silicon flow sensors for gas flow meters," *Sensors and Actuators*, A 54, pp.626-631.

[7] Lammerink, T.S.J., Tas, N.R., Elwenspoek, M. and Fluitman, J.H.J., 1993, *Sensors and Actuators*, A 37-38, pp.45-50.

[8] Makinwa, K.A.A. and Huijsing, J.H., 2002, *Sensors and Actuators*, A 97-98, pp.15-20.

[9] Chung, W.Y., Lim, J.W. and Lee, D.D., 2002, *Sensors and Actuators*, B 83, pp.281-284.

[10] Okulan, N. and Henderson, H.T., 2000, *IEEE Trans. On Electron Devices*, Vol.47, No.2, pp.340-347.

[11] Kawamura, T. and Kuwahara, K., 1985, *AIAA 23rd Aerospace Sciences Meeting*, January 9-12, pp.1-10.

[12] Kawamura, T. and Kuwahara, K., 1984, *AIAA 22nd Aerospace Sciences Meeting*, January 14-17, pp.1-11.